Experimental and numerical study of a latent heat storage using sodium acetate trihydrate for short and long term applications

Wang, Gang; Xu, Chao; Englmair, Gerald; Kong, Weiqiang; Fan, Jianhua; Furbo, Simon; Wei, Gaosheng

Published in:
Journal of Energy Storage

Link to article, DOI:
10.1016/j.est.2021.103588

Publication date:
2022

Document Version
Version created as part of publication process; publisher's layout; not normally made publicly available

Journal of Energy Storage xxx (xxxx) xxx

Contents lists available at ScienceDirect

Journal of Energy Storage

journal homepage: www.elsevier.com/locate/est

Research Papers

Experimental and numerical study of a latent heat storage using sodium acetate trihydrate for short and long term applications

Gang Wang [a,b], Chao Xu [a], Gerald Englmair [b], Weiqiang Kong [b], Jianhua Fan [b,*], Simon Furbo [b], Gaosheng Wei [a]

[a] Key Laboratory of Condition Monitoring and Control for Power Plant Equipment of MOE, North China Electric Power University, Beijing 102206, P R China
[b] Department of Civil Engineering, Technical University of Denmark, Brovej 118, Kgs. Lyngby 2800, Denmark

ARTICLE INFO

Keywords:
Phase change material
Flexible heat storage
Experiments
CFD simulation
Thermal characteristic

ABSTRACT

A flexible thermal energy storage with 137.8 kg PCM and 75 L water was introduced. The heat storage combined short-term and long-term heat storage functions by utilizing sodium acetate trihydrate as heat storage material. The thermal performance and flow characteristics of the heat storage were investigated by experiments and by CFD simulations. The result show that after a full charge to 92 °C, the heat storage can flexibly release heat in two steps: In the first step, 13.7 kWh sensible heat can be released for short-term use; in the second step, 7.8 kWh latent heat can be released for long-term use. When releasing heat, there is laminar flow of water and a high degree of thermal stratification in the tank. During discharge of the sensible heat, the heat storage can provide 294 L hot water with an average temperature of 68.2 °C. During discharge of the latent heat, 334 L hot water with an average temperature of 46.7 °C were drawn from the heat storage. In the charging process, a fluid short circuit existed inside the water region. Part of hot water flows out of the tank before sufficiently heated. There was no obvious thermocline inside the tank during charging. The flow rate has a big influence on the thermal characteristics of the heat storage during the charge and discharge periods. By increasing the flow rate from 4 L/min to 14 L/min, the charging time was shortened by 67% from 276 min to 92 min while the discharging time was shortened by 65% and 83% respectively in releasing sensible heat and latent heat.

1. Introduction

As the awareness of environmental protection gradually increase, renewable energy is going to be the primary energy source in the future, and there is a significant global trend that the energy supply will have to switch to energy from renewable sources [1]. Many investigations have been carried out to provide secure, affordable and renewable energy sources [2]. One of the key renewable energy sources is solar energy [3]. Increasing the usage of solar energy can reduce the emission of carbon dioxide, provide more energy supply diversification and increase regional energy independence [4]. To provide a stable solar energy supply, adding an energy storage system is a key point to solve the discontinuity of solar energy.

Energy storage refers to a process that excess energy is stored into a form that can be transferred back to the same form or a different form when needed [5]. Thermal energy storage (TES) is the main energy storage technology due to its low cost, security and flexibility. With TES systems, the efficiency and reliability of energy systems will be improved significantly [6].

1.1. Water-PCM short-term heat storage

Short-term heat storage can realize the peak load shifting of heat demand. The most commonly used short-term heat storage method in engineering is water heat storage technology. The domestic solar water tank is the cheapest method to store solar thermal energy for domestic hot water supply, the most common usage of solar thermal energy is solar water heaters in residential and commercial use [7].

Latent heat storage has many advantages, such as high energy storage density and smaller temperature changes during charge and discharge processes [8,9]. Latent heat storage has been used as short-term heat storage. When adding phase change material (PCM) in short-term heat storage, the thermal storage density of the TES system is significantly increased due to the high latent heat of PCM [10]. But until now, systems with PCM used as the main energy storage material are rare. The low thermal conductivity [11] and the price of PCM [12] limit the application of using PCM as heat storage materials.

* Corresponding author.
E-mail address: jif@byg.dtu.dk (J. Fan).

https://doi.org/10.1016/j.est.2021.103588
Received 12 August 2021; Received in revised form 16 October 2021; Accepted 5 November 2021

Nomenclature

ρ	density [kg/m^3]
t	time [s]
$\vec{v}$	velocity [m/s]
μ	viscosity [Pa·s]
P	pressure [Pa]

bbreviations

PCM	phase change material
CFD	computational fluid dynamics
TES	thermal energy storage
HTF	heat transfer fluid
$\vec{g}$	gravity [m/s^2]
β	liquid volume fraction
H	enthalpy [J, kWh]
L	latent heat [J/(kg·K)]
T	temperature [K, °C]
HXCR	heat exchange capacity rate
RE	relative energy
DHT	direct heating tubes

The typical approach is to add PCM to traditional short-term heat storage to increase the thermal performance of the heat storage system [13]. Shalaby et al. [14] added PCM in a domestic water heat storage for single-family houses, the heat storage can provide hot water (>50 °C) during a day. Lamrani et al. [15] evaluated the feasibility of adding PCM in the solar water heater for large buildings' hot water production. The results show that under the weather condition of south France, the water-PCM heat storage is suitable for large buildings' hot water production, the produced hot water was within the ranges of 85–36 °C and 63–38 °C during daytime and nighttime respectively. Qin et al. [16] proposed a case of adding PCM to improve the thermal performance of a 60 L hot water tank. The results show that after adding PCM, the heat storage density of the tank was 84.4 kWh/m^3 (from 5 to 80 °C). Placing PCM at a low position can accelerate the heat release.

1.2. Long-term heat storage

Long-term heat storage allow flexibe integration of various fluctuating renewable energy sources [17]. Long-term heat storage is the key technique to solve the seasonal mismatch between energy supply and demand [18].

Water pit heat storage has been utilized as a seasonal heat storage system. Large solar district heating plants with water pit long-term heat storage have developed very fast in the last decade in Denmark [19]. The first water pit heat storage of 10,000 m^3 was demonstrated in Marstal in 2004. Then water pit storages with improved designs were constructed in Marstal (75,000 m^3, 2012) [20], Dronninglund (62,000 m^3, 2014) [21] and Vojens (203,000 m^3, 2015) [22].

PCM can also be used in long-term heat storage utilizing stable supercooling of liquid PCM [23,24]. With stable supercooling, latent heat can be kept at room temperature for a long period with low heat losses. Experiments at the Technical Unversity of Denmark showed that stable supercooling of SAT-based PCM in a small tank was successfully kept for more than 2 years [25]. And then the heat loss of long-term heat storage utilizing stable supercooling is relatively low [26].

Cylindrical heat storage with 116 kg PCM was tested by Dannemand et al. [27]. The measured energy storage density of the heat storage was 110 kWh/m^3 (from 20 to 90 °C). But only in 6 of 40 experiments the cylindrical PCM heat storage achieved stable supercooling for long-term heat storage. A segmented heat storage prototype utilizing PCM stable supercooling for long-term heat storage was investigated by Englmair et al. [28]. In the discharge process, the units released 30.6–34.2 MJ sensible heat first. After discharging sensible heat, the latent heat was still stored in the supercooled SAT in the prototype. The latent heat was released after triggering the solidification of the supercooled PCM. In the experiments, 31.7–37.1 MJ latent heat was released from the prototype.

1.3. Numerical investigations of PCM heat storages

Commercial software is commonly used in the numerical investigations of PCM. Trnsys and CFD are two popular commercial software. Trnsys is usually used for system analysis of TES systems with PCM heat storage. CFD is usually used for the thermomechanical analysis of PCM heat storage.

The performance of solar heating systems with heat storage utilizing stable supercooling of SAT has been successfully investigated and predicted by Trnsys and Matlab simulation. Dannemand et al. [29] simulated a solar heating system with flat long-term SAT heat storage and 36 m^2 solar collectors using a new Trnsys type. A multiple flat PCM heat storage Trnsys model-Type 8888 was developed by Graz University of Technology. A solar heating system for a single family house with the flat SAT heat storage [28] was simulated in Trnsys using Type 8888 under Danish climate conditions [30].

Mohammadnejad et al. [31] investigated the influence of different alignments of PCM packed beds on the total thermal performance of the TES system, but the supercooling degree was ignored in the research. Bouhal et al. [32] simulated the melting process of a PCM filling a cylindrical cavity which includes heating sources. Only the melting process was considered, discharging and solidification were not simulated. Pawar et al. [33] performed a three-dimensional transient CFD modeling of an evacuated heat pipe tube solar collector system with PCM using ANSYS Fluent 19. Both melting and solidification were simulated, but the supercooling degree was not considered. Dannemand et al. [34] performed a simulation using CFD to investigate the thermal performance of a SAT heat storage, also the supercooling of SAT was ignored. The supercooling characteristic of PCM is still a problem for numerical study. A CFD considering supercooling characteristic is imperative to present the accurate results of PCM heat storage.

1.4. Aim and scope

In the current energy market, short-term heat storage has been widely used. The long-term heat storage, due to its long earning cycle and large space occupation, is still in the early stage. Flexible heat storage combining short-term and long-term heat storage is proposed in this research for green buildings and renewable energy systems. The flexible heat storage was designed and constructed by H.M. Heizkörper, and 137.8 kg PCM and 75 L water were filled in the heat storage.

This research is part of the Danish Energy Agency EUDP project on participation of the IEA Task 58 'Material and Component Development for Thermal Energy Storage'. In this investigation, the proposed flexible thermal energy storage was investigated for the first time by experiments and CFD simulation. The thermal characteristic of the heat storage was investigated in the experiments and the flow characteristics were revealed by CFD simulations. The flow characteristics of water were revealed to evaluate the thermal performance of the heat storage. The melting characteristic was also revealed to show the phase change process of the PCM inside the heat storage. The influence of flow rate on the thermal characteristics of the heat storage will be determined.

2. Experimental setup

2.1. Design of the PCM heat storage

A photo of the heat storage is presented in Fig. 1. The height of the storage is 1.7 m, and the outer diameter is 0.4 m (without insulation). 112 tubes are mounted vertically inside the storage, see Fig. 2 and Fig. 3,

Fig. 1. The heat storage unit without insulation.

Fig. 2. The manifold plate with a view of the tubes inside the storage (PCM was melted).

each with a length of 1.52 m and an inner diameter of 0.0276 m. The tops of the tubes are fixed to a stainless steel plate and open to the volume above the plate. The inlet of the heat storage is located at the bottom of the storage, and the outlet is located at the top of the storage water volume under the stainless steel plate. The inlet and outlet are placed on opposite sides of the tank. The tank was covered by an insulation layer of 30 mm mineral wool. Fig. 2 shows the top structure of the storage and Fig. 3 shows the structure of the storage. More details of experimental investigation can be found in the previous publication [26].

The storage was built with 166 kg stainless steel, the shell contained 75 L water as heat transfer fluid surrounding the tubes with PCM. The

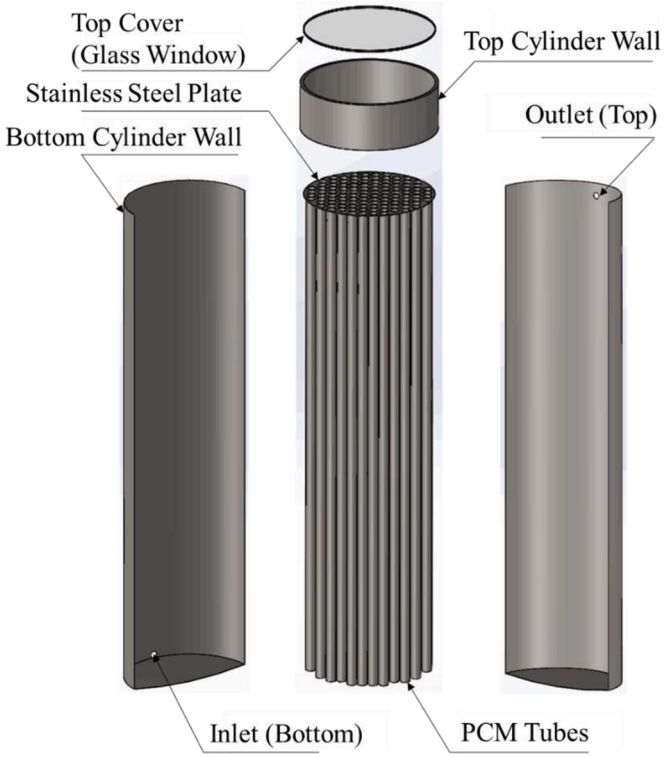

Fig. 3. A break-down drawing of the heat storage.

heat transfer area between water and PCM, i.e. the outside surface of the immersed part of the tubes was 16.2 m^2. The tubes were filled with 137.8 kg PCM developed by HM Heizkörper GmbH Heating Technology.

2.2. PCM material

The PCM is a patented SAT-based composite with liquid polymer and extra water. The melting point of the PCM is between 53 and 58 °C, the latent heat is in the range of 205–210 kJ/kg. The properties of the PCM used in CFD calculations are listed in Table 1. Besides the PCM properties, the properties of water and stainless steel are directly selected from the Fluent Material Database.

2.3. Experiment procedure

Before every test, the heat storage was kept in a stable state. The initial temperature of the storage was uniform. During charging, the inlet temperature was set to 92 °C and the test period was 20 h. During discharging of sensible heat and discharging of latent heat tests, the inlet temperature was 30 °C and the test period was 10 h. The solidification of supercooled PCM was triggered by dropping SAT crystals. The discharging of latent heat test lasted for 10 h. In all tests, the flow rate was kept at 7 L/min. The end of the charging and discharging process was defined by the temperature difference between inlet temperature and

Table 1
The PCM thermal properties.

Properties	Values	Units
Melting temperature	53	°C
Latent heat	209	kJ/kg
Solid specific heat capacity	2840	J/(kg·K)
Liquid specific heat capacity	3020	J/(kg·K)
Density of solid	1341	kg/m^3
Solid thermal conductivity	0.55	W/(m·K)
liquid thermal conductivity	0.34	W/(m·K)
Thermal expansion coefficient	0.000512	1/K

outlet temperature. If the temperature difference is stable, the charging and discharging process was considered as completed.

Fig. 4 shows a diagram of the heat storage test rig. SAT was filled in the PCM tubes and in the upper part of the heat storage. The heat transfer fluid, water, enters into the bottom of the tank and flows in between the PCM tubes before exiting the heat storage. Ten thermocouples were placed on the outer surface of the cylindrical tank in good thermal contact with the tank wall and covered by the insulation. Two thermocouples were placed in inlet and outlet to determine the inlet and outlet temperature. The type of used thermocouples were TT-type with a maximum measuring uncertainty of 0.5 K [35]. A five junction thermopile with an uncertainty of 0.1 K was used to measure the temperature difference between the in- and outlet of the heat transfer fluid.

3. CFD model and methodology

An ANSYS 19.2 CFD model of the PCM heat storage was developed [36]. The structured mesh was adopted in this model (totally 1.38×10^6 cells), the mesh skewness of the model was 0.64. To ensure the accuracy of the simulations, the boundary layers were added in the model both inside and outside of the tubes. The CFD model was imported into Fluent to carry out the numerical simulations. Fig. 5 shows the generated mesh.

3.1. The governing equations

The CFD model is developed to study the effects of different flow rates and temperatures of the heat transfer fluid (HTF) on the charging, supercooling and discharging processes of the heat storage. For the simulation process solver equation, the following assumptions are considered:

- The working fluid (both PCM and HTF) is incompressible.
- The crystallization occurred simultaneously in the whole volume.
- The thermophysical properties of PCM are independent of temperature.
- The volume of PCM does not change in the phase change process.

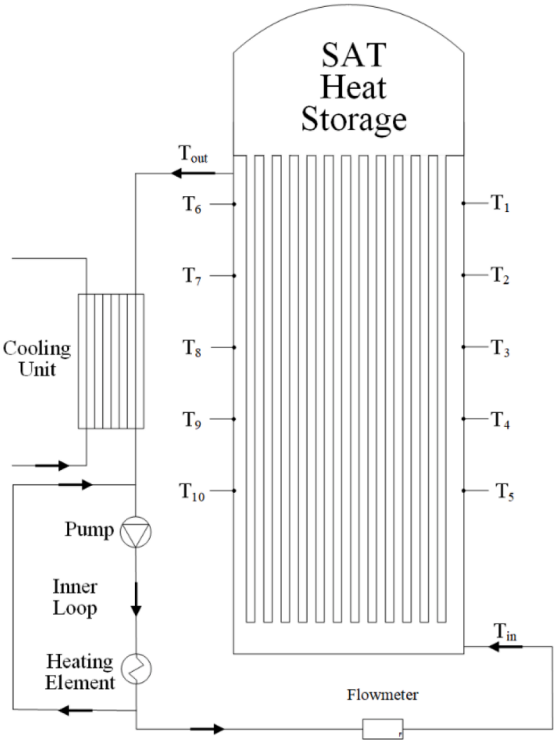

Fig. 4. Principle sketch of heat storage in the testing facility [26].

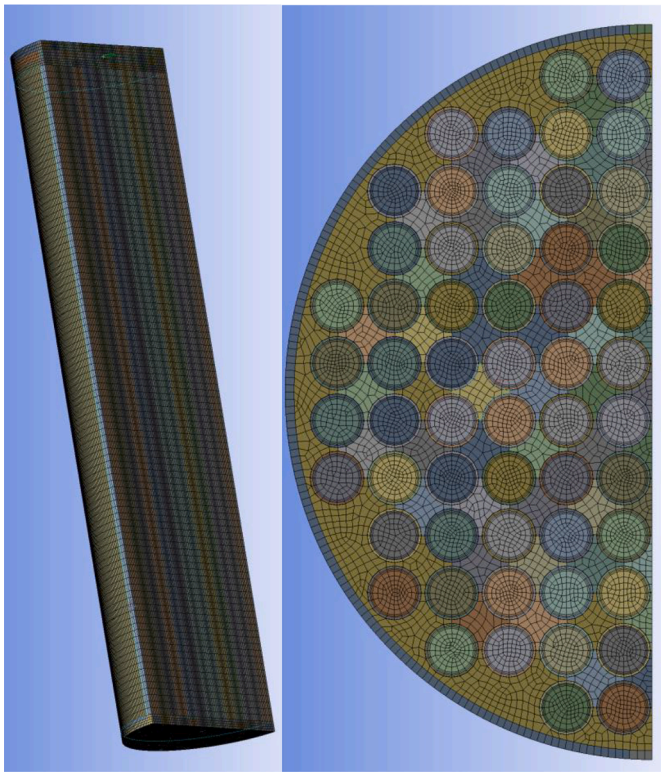

Fig. 5. The generated mesh used in CFD simulation (left: vertical middle cut plane, right: horizontal cut plane).

The governing equations of the solidification and melting model are [37]:

Continuity equation:

$$\frac{\partial \rho}{\partial t} + \nabla \cdot (\rho \vec{v}) = 0 \tag{1}$$

Momentum equation:

$$\frac{\partial}{\partial t}(\rho \vec{v}) + \nabla \cdot (\rho \vec{v}\,\vec{v}) = \mu \nabla \cdot \vec{v} - \nabla P + \rho \vec{g} + S \tag{2}$$

where S is the momentum source term due to the reduced porosity in the mushy zone and can be expressed as:

$$S = \frac{(1-f)^2}{\left(f^3 + \varepsilon\right)} A_{\text{mush}} \vec{v} \tag{3}$$

where f is the liquid volume fraction, ε is a small number (0.001) to prevent division by zero, A_{mush} is the mushy zone constant.

Energy equation:

$$\frac{\partial}{\partial t}(\rho H) + \nabla \cdot (\rho \vec{v} H) = \nabla \cdot (k \nabla T) \tag{4}$$

where H is enthalpy, ρ is density, $\vec{v}$ is fluid velocity.

H is computed as the sum of the sensible enthalpy h, and the latent heat ΔH,

$$H = h + \Delta H \tag{5}$$

The latent heat content can now be written in terms of the latent heat of the material L:

$$\Delta H = fL \tag{6}$$

where f is the liquid fraction, which can be defined as:

$$\begin{aligned} &f = 0 && if \quad T < T_{solidus} \\ &f = 1 && if \quad T > T_{liquidus} \\ &f = \frac{T - T_{solidus}}{T_{liquidus} - T_{solidus}} && if \quad T_{solidus} < T < T_{liquidus} \end{aligned} \tag{7}$$

where $T_{solidus}$ is the temperature of the PCM when the last liquid content is solidified and $T_{liquidus}$ is the temperature of the PCM when the last solid content is liquified.

The effect of natural convection during melting was considered, and the Boussinesq approximation was used to calculate the buoyancy-driven forces [38]. The governing equations were solved in a pressure-based transient solver. The gravity was considered (9.8 m/s^2). Under all inlet conditions, the Reynolds number and Rayleigh number show that the flow of HTF outside the tubes and the flow of liquid PCM inside the tubes are both laminar flow. The laminar model was adopted in the simulation. The PISO algorithm was employed for the pressure–velocity coupling, and the PRESTO and second-order upwind method were used to discretize the pressure and the momentum/energy equations, respectively. The predetermined convergence criteria for continuity, velocity and energy were 10^{-3}, 10^{-3}, and 10^{-6} respectively. Three time step sizes 0.05 s, 0.1 s and 0.2 s were used, the results showed that there was almost no difference when using different time steps. To maximum the calculation efficiency, 0.2 s was selected as the time step size in all simulations.

3.2. Boundary conditions

In all simulations, the inlet flow rates and inlet temperatures were constant (based on simulation conditions). The outlet was set to outflow type. The heat loss coefficient of the heat storage was determined by experiment in the previous study [26] and used as input in the CFD model. The effective heat transfer coefficient of the heat storage surface was 1.7 W/(m^2·K).

3.2.1. Thermal characteristic determination

In this part, the boundary conditions were the same as the experimental conditions. Before each test, the model was initialized with uniform temperature. For the charging process and discharging of latent heat process, the initial temperature was 30 °C. For discharging of the sensible heat process, it was 92 °C.

During the charging, the discharging of sensible heat and the discharging of latent heat tests, the inlet temperature was set to 92, 30 and 30 °C respectively, same as the values in the experiment. The solidification of supercooled PCM was triggered in discharging of the latent heat process. In all processes, the flow rate was kept at 7 L/min.

3.2.2. Effect of inlet flow rate

The influence of different inlet flow rates on the thermal performance of the heat storage was investigated after determining the thermal characteristics of the heat storage. Four different flow rates 3 L/min, 7 L/min, 10 L/min and 14 L/min were used in all three processes. Except for the inlet flow rate, other conditions were kept same.

3.3. Data analysis

The change of heat content (HC) during a time step of Δt was determined by Eq. (8):

$$\Delta HC = (P_{in} - P_{out} - P_{heatloss}) \cdot \Delta t \tag{8}$$

P_{in}, P_{out} and $P_{heatloss}$ is the heat transfer rate [W] at inlet, outlet and tank surface respectively.

It was assumed that $HC = 0$ when the heat storage temperature is 30 °C.

The power (P) transferred to or from the heat storage was determined by Eq. (9):

$$P = P_{in} - P_{out} \tag{9}$$

The heat exchange capacity rate ($HXCR$) was determined by Eq. (10):

$$HXCR = -\, c_{p.water} \cdot \rho_{water} \cdot \dot{V} \cdot ln\left(1 - \frac{T_{in} - T_{out}}{T_{in} - T_{average}}\right) \tag{10}$$

4. Results and discussion

4.1. Model validation

The SAT heat storage can be used to store heat in short terms (several days) or long terms (several months), which, as an advantage, gives flexibility for the energy system. When used as a short-term heat storage, the SAT should melt or crystalize at the phase change temperature, resulting in storage and release of thermal energy. While as a long-term heat storage, the SAT has the ability to stably supercool of up to 80 K, thus, storing heat as heat of fusion for months without additional heat losses. In order to evaluate thermal performance of the heat storage for short-term or long-term uses, the following scenarios were investigated:

- Charging process (relevant for short and long-term heat storage)
- Discharging with sensible heat (for short-term heat storage)
- Discharge with latent heat (for long-term heat storage)

The model was validated by comparing the outlet temperature measured and calculated. In the experiment, the inlet temperature was not constant, since it increased or decreased gradually from the initial state to the final state. The measured inlet temperature was used in the simulations. Fig. 6,7,8 shows the comparison between measured and calculated outlet temperatures and discharged/charged heat.

For the charging process, calculated outlet temperatures and charged heat have the same trend as the measured ones. The measured and calculated outlet temperature started at 30 °C, and after 450 min, the measured outlet temperature and the calculated outlet temperature ended at 91 °C. During the start period (0–15 min) and the end period (270–450 min) of the test, the difference between the calculated and measured outlet temperatures was less than 2 K. From 110 min to 190 min, the calculated outlet temperature was lower than the measured outlet temperature. The maximum difference is 3 K, which occurred at 144 min. For the charged heat, during the whole process, the calculated and measured values were in a good agreement. When the heat storage was fully charged, the calculated heat transfer to the heat storage was 22.1 kWh, which was 0.4 kWh (1.8%) higher than the measured result.

For discharging of the sensible heat, the heat storage released 13.7 kWh heat to the water which was then transferred out of the heat storage. The calculated results were very close to the measured results. The differences between the calculated and measured results were less than 0.7% for energy and 2 K for temperature.

For discharging of the latent heat process, the solidification of supercooled PCM was achieved successfully by the CFD model. The calculated results had the same outlet temperature increase as the measured results during this process. The heat storage released 7.8 kWh latent heat to the water. Concerning the released heat during this process, before 80 min, the difference between the simulation and the experiment was less than 0.1 kWh (1.5%). After 100 min, the calculated heat was slightly higher than the measured result, but the maximum

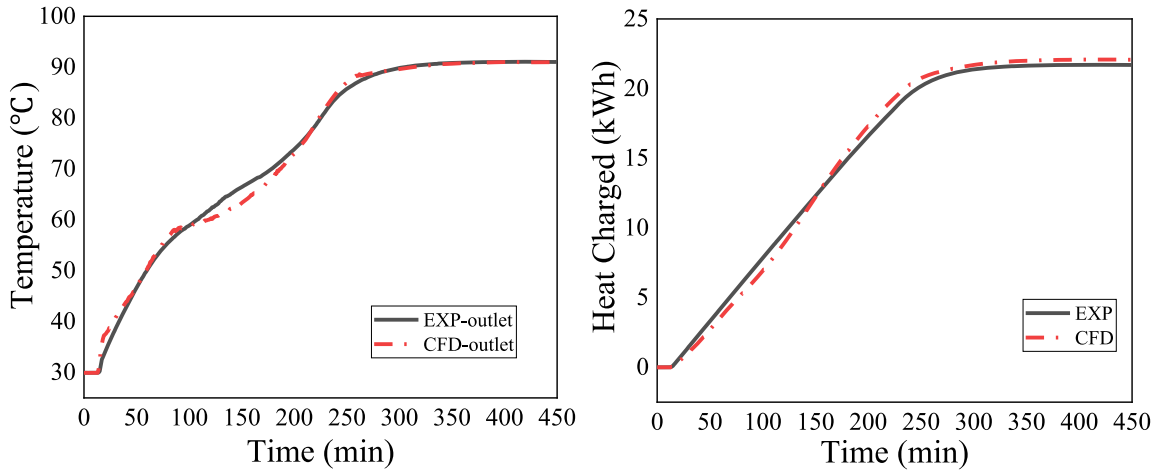

Fig. 6. Comparison between calculations and measurements during the charging process.

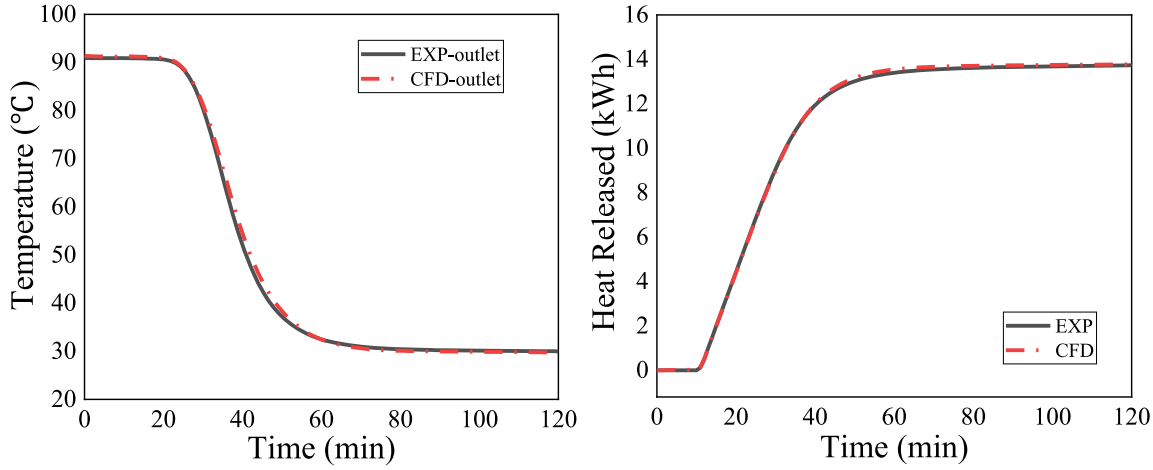

Fig. 7. Comparison between calculations and measurements during discharging of sensible heat process.

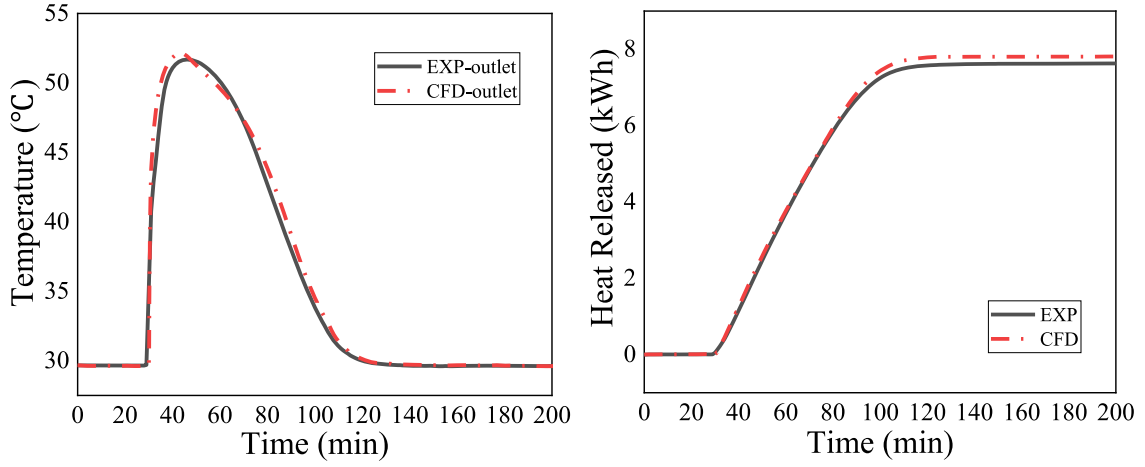

Fig. 8. Comparison between calculations and measurements during discharging of latent heat process.

difference was less than 0.3 kWh (2.5%).

Based on the comparison, the accuracy of the CFD model was verified, and the CFD model can be considered to be acceptable for the following analysis.

4.2. Water flow characteristics

4.2.1. Charge

Fig. 9 shows the water flow pattern inside the heat storage tank in the charging process. During charging, the initial temperature of the tank was 303 K (30 °C), the inlet water temperature was 365 K (92 °C), and

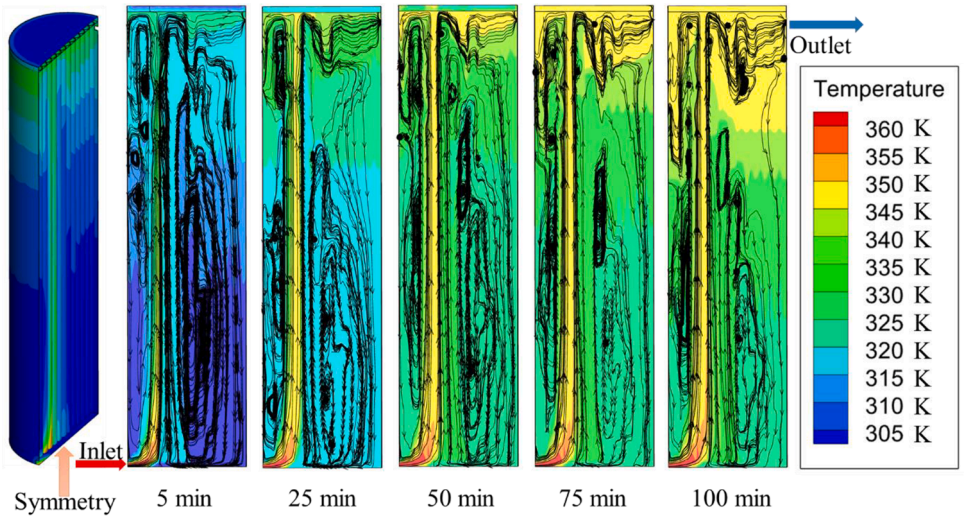

Fig. 9. The water flow pattern inside the heat storage during charge.

the flow rate was 4 L/min. The hot water came in from the inlet with horizontal velocity (from left to right). Due to water resistance, the horizontal velocity gradually decreased to 0 m/s. However, the vertical velocity of hot water increased due to buoyancy. At the top of the tank, hot water reached the top plate, part of hot water flow to the left side and then flows down the wall; part of hot water flows to the right side. Through the outlet, cold water with part of hot water flows out of the tank.

As hot water rises in the tank, the nearby cold water was carried upward and heated by the hot water, but its velocity and temperature were smaller than that of the hot water. When upward cold water reached the warm region (top of the tank), it changed from upward to downward. From Fig. 9, the reverse flow of water can be found between hot water and the tank surface. As the charging process goes on, temperature of the water increased. The temperature difference between hot water and cold water decreased, the buoyancy driving force decreased, and then the reverse flow was weakened.

During charging, the hot water was not mixed well before rising. And inside the tank, a fluid short circuit existed, part of the hot water directly flows out of the tank before totally released its heat. In this case, thermal stratification was formed inside the tank and the temperature of the top part was higher than that of the bottom part. A fluid short circuit of hot water reduced the charging power and heat exchange capacity rate of the tank.

4.2.2. *Discharge of the sensible heat*

Fig. 10 shows the water flow pattern inside the heat storage in the process of discharging of the sensible heat. During this process, the initial temperature of the tank was 365 K (92 °C), the inlet water temperature was 303 K (30 °C), and the flow rate was 4 L/min.

The cold water entered the tank horizontally. Due to its relatively low temperature, cold water flows along the bottom surface and does not move upwards. When cold water hit the opposite inner tank wall (outlet side), it changed flow direction. Part of the cold water flows along the side wall and back to the inlet side, before mixing with the fresh inlet cold water. The rest of the cold water flow upward along the side wall. In general there was a regular uprising flow in the heat storage. No strong short circuit can be observed inside the tank. The thermal stratification inside the tank was obviously good. The influence of the above mentioned reverse flow was limited. As shown by the flow pattern, the performance of the tank during discharging of sensible heat was satisfactory.

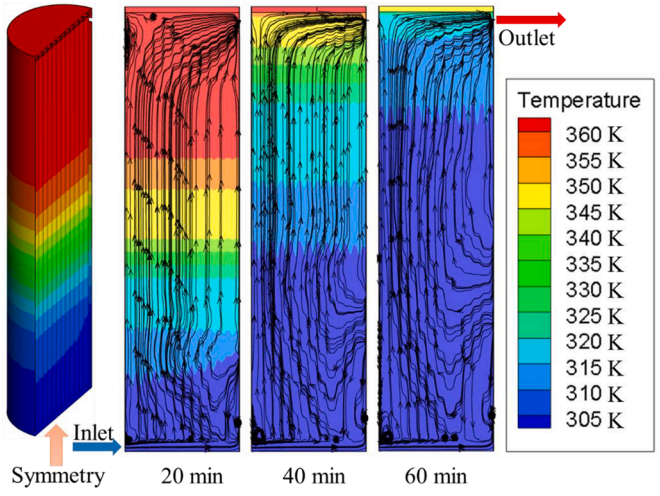

Fig. 10. The water flow pattern inside the heat storage during discharge of sensible heat.

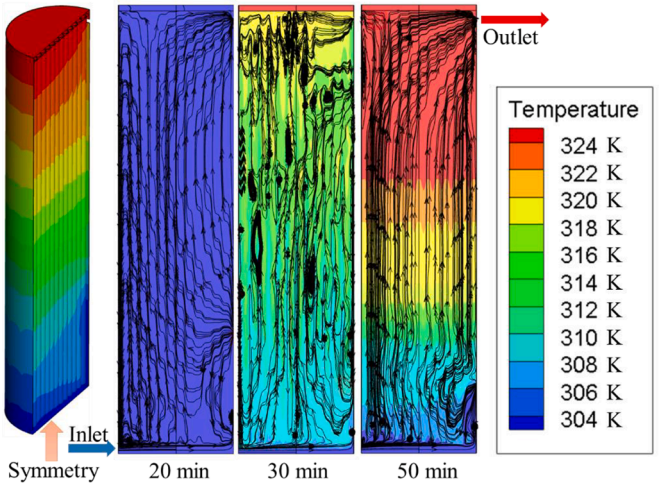

Fig. 11. The water flow pattern inside the heat storage during discharge of latent heat.

4.2.3. Discharge of the latent heat

Fig. 11 shows the water flow pattern inside the heat storage in the process of discharging of latent heat. The initial temperature of the tank was 303 K (30 °C), the temperature of the cold water supply was 303 K (30 °C), and the flow rate was 4 L/min. Before discharging, the PCM was kept in a stable supercooling state in the tubes with a temperature of 30 °C. The latent heat of PCM was released at 20 min after the start by triggering the solidification of supercooled PCM. Consequently, temperature of the PCM increased from 303 K to 326 K. Water inside the tank was heated by the warm tubes. The maximum temperature of the water reached around 326 K. After triggering the solidification of PCM, the water flow pattern in the tank was similar to that during discharging of the sensible heat.

4.3. Melting characteristic of PCM

The PCM inside the tubes melted during the charging process. The melting characteristic is discussed in this section. The third row of tubes (A-A) was selected for analyzation since they were not directly influenced by the gathered hot water, see Fig. 12. Fig. 13 shows the heat exchange capacity rate (*HXCR*) of the tank during charging vs. relative energy. The relative energy (RE,%) is defined as the ratio between the absorbed/released energy and the maximum absorbed/released energy of the tank. RE gives a good indication on how far the charging stands. The data of relative energy less than 10% and more than 90% was deleted to ignore the inaccuracy during the start and the end of charging.

From Fig. 12 and Fig. 13, the melting of PCM started from the location close to the inner wall of tubes. When PCM started melting, a lot of heat was absorbed and stored as latent heat in PCM. The temperature of melting PCM was kept at the melting point, but the temperature of the wall of the tube increased. The temperature difference between the wall and melting PCM increased, resulting in that the *HXCR* of the tank increased from 607 W/K to 779 W/K (RE from 10% to 23%).

After the PCM close to the wall finished melting, the melting interface moved toward the center of the tube. Because of the small volume of melted PCM, there was almost no sign of convection inside liquid PCM. Heat was transferred from the wall to unmelted PCM by thermal conduction. Since the thermal conductivity of liquid PCM was smaller than that of solid PCM, *HXCR* decreased with the increase of liquid PCM, from 779 W/K to 390 W/K (RE from 23% to 60%).

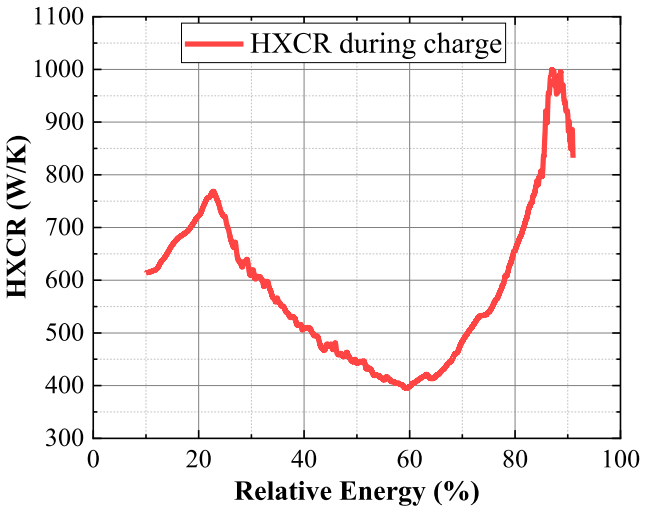

Fig. 13. The *HXCR* of the tank during charging.

With the increase of liquid PCM, the volume of liquid PCM was large enough to form convection. After the formation of convection, the heat transfer of the tank was enhanced obviously, the *HXCR* increased from 390 W/K to 1000 W/K (RE from 60% to 88%). And then, after most PCM finished melting, the temperature of liquid PCM increased rapidly. The temperature difference between hot water and liquid PCM was decreased, resulting in *HXCR* decreased from 1000 W/K to less than 830 W/K.

4.4. The influence of inlet flow rate

4.4.1. Melting process of PCM inside the tank

Fig. 14 shows the influence of different inlet hot water flow rates on the temperature distribution on the tank symmetry plane.

During charging, the incoming hot water was not uniformly distributed inside the tank, instead it gathered in a certain region inside the tank. The temperature of the hot water region was higher than the

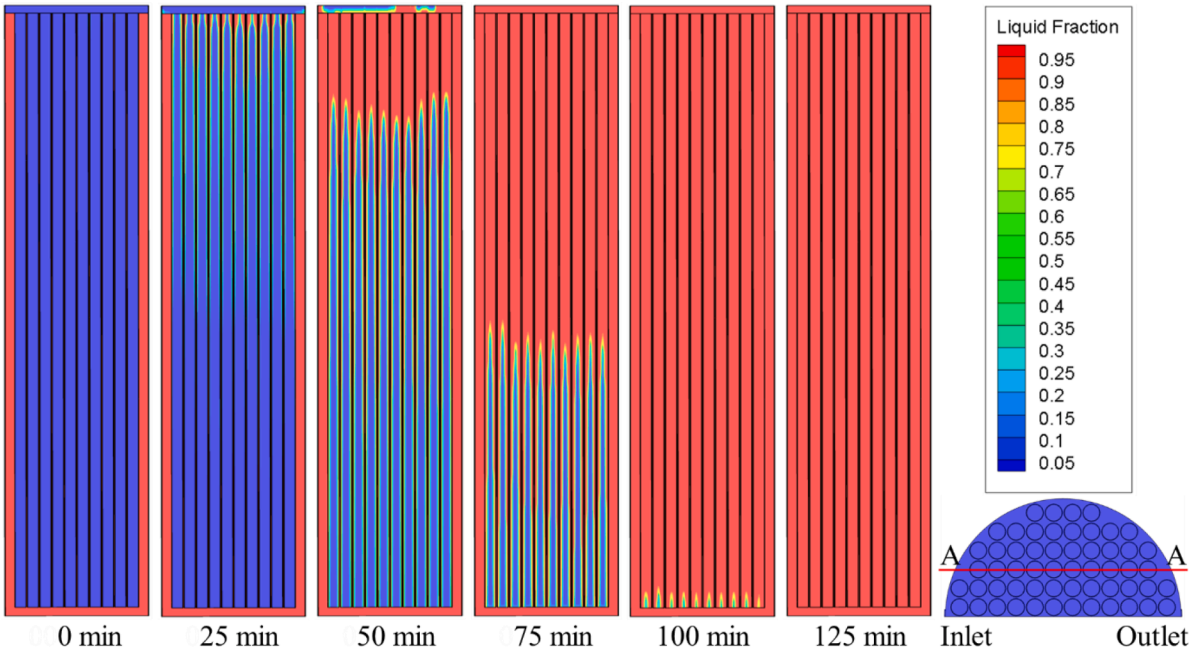

Fig. 12. The distribution of liquid fraction on A-A cross-section during charge.

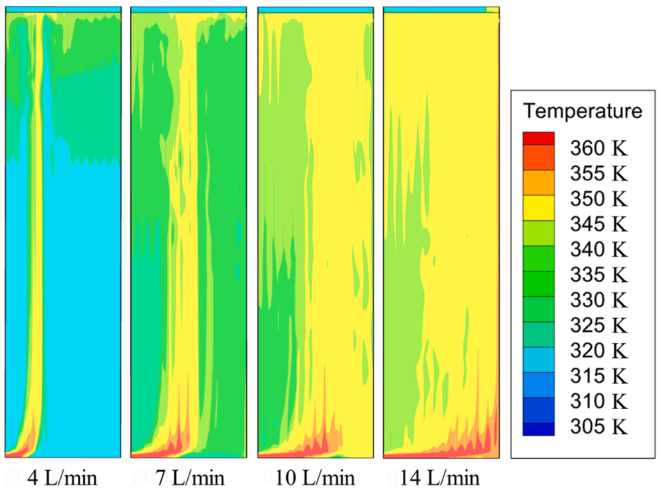

Fig. 14. Temperature distribution of the symmetry plane under different inlet flow rates.

temperature in the other parts of the heat storage. Therefore, the PCM tubes were not heated uniformly. The tubes in the hot water region were directly heated, these tubes were called Directly Heated Tubes (DHT). The other tubes were heated by the convection inside the tank, these tubes were called Generally Heated Tubes.

The location of the DHT region was close to the inlet side when the flow rate was low, and when it was high, the region was close to the outlet side. The area of the DHT region increased with the increase of flow rate. Compared with the low flow rate conditions, independent of the tank size, the amount of DHT in the high flow rate conditions was greater, meaning that more tubes could be heated rapidly.

To achieve stable supercooling, it is crucial to make sure that all SAT in the heat storage is melt completely during charging. Failure to do it will cause spontaneous crystallization of SAT and unwanted release of latent heat. Fig. 15 shows the minimium time needed to completely melt the PCM in the tube. The initial temperature of the tank was 303 K (30 °C) and the temperature of inlet hot water was 365 K (92 °C) under all four conditions. From Fig. 13, DHT was distributed only in the first row close to the symmetry plane, meaning the area of the hot water region was narrow, and the situation was not significantly changed with the increase of the flow rate.

With the increase of the flow rate, the difference between the longest t_{tfm} and the shortest t_{tfm} decreased. For 4 L/min, the difference was 78 min while for 7 L/min, it was 27 min and for 10 L/min was 15 min. However, due to the limitation of the tank size, for 14 L/min, the difference was 21 min. If ignoring the limitation of the tank size, the higher inlet flow rate would result in a more uniform heat transfer rate.

Fig. 16 shows the calculated melting and charging time of the tank. Both the melting time and the charging time decreased with the increase of flow rate. The decrease rate of the melting time decreased with the increase of flow rate. This means increasing the flow rate can indeed enhance the heat transfer of the heat storage. But the effect decreases with the increase of the flow rate.

4.4.2. *Influence of flow rates on thermal characteristics*

Ideally, the SAT heat storage is used to store renewable heats, for example, solar heat. Integration with solar heat requires that heat exchange capacity rate (*HXCR*) of the heat storage is sufficiently high (> 400 W/K) [26]. It is therefore crucial to investigate how power and *HXCR* of the heat storage are influenced by the flow rate of the heat transfer fluid.

4.4.2.1. Charge. Fig. 17 shows the power and *HXCR* of the tank under different flow rate conditions during charge. Under four flow rate

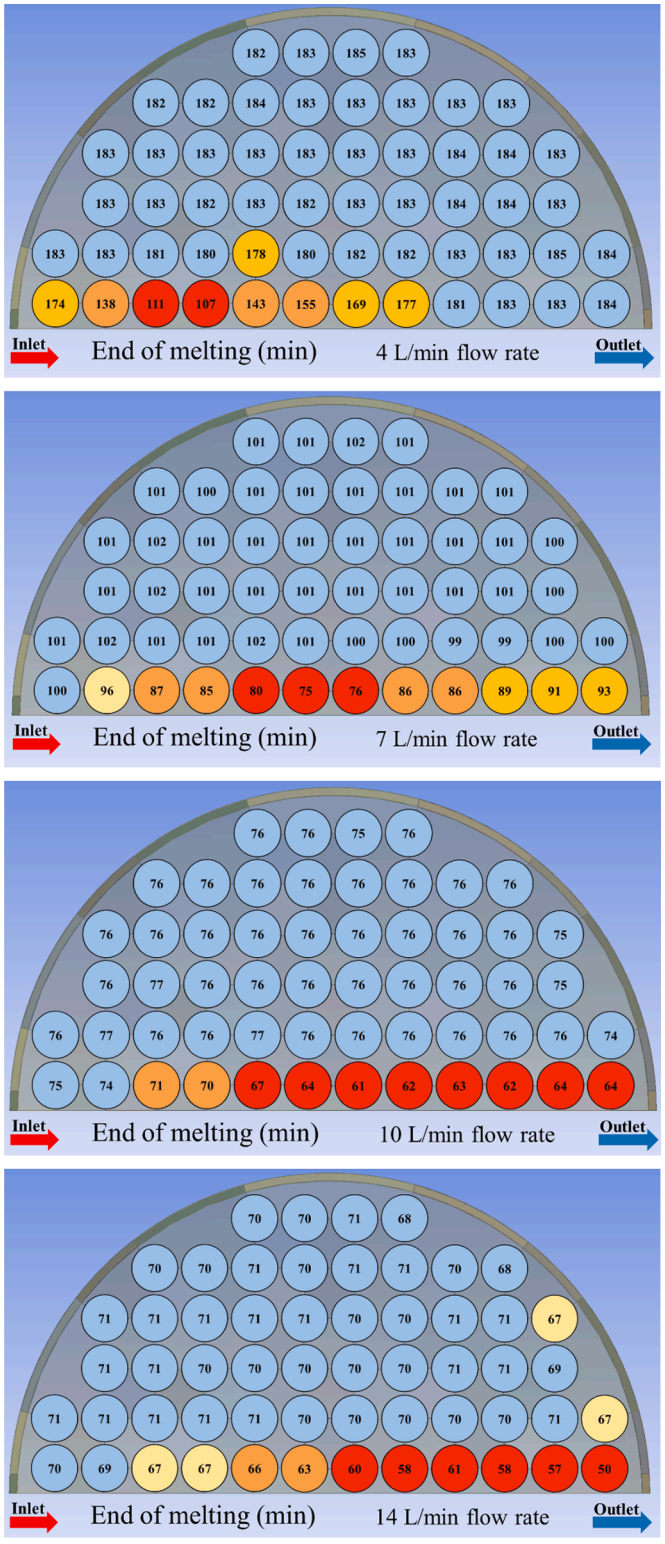

Fig. 15. Distribution of the minimum time needed for complete melting of the PCM under different flow rate conditions.

conditions, power decreased with the development of the charge. When the flow rate increased from 4 L/min to 7 and 10 L/min, the power increased significantly. But when the flow rate increased from 10 L/min to 14 L/min, the increase of power was not obvious. A similar phenomenon was also found for *HXCR*. The *HXCR* increased by increasing the flow rate. However, when the flow rate was 14 L/min, the *HXCR* was lower than for 10 L/min. This means the heat transfer inside the tank

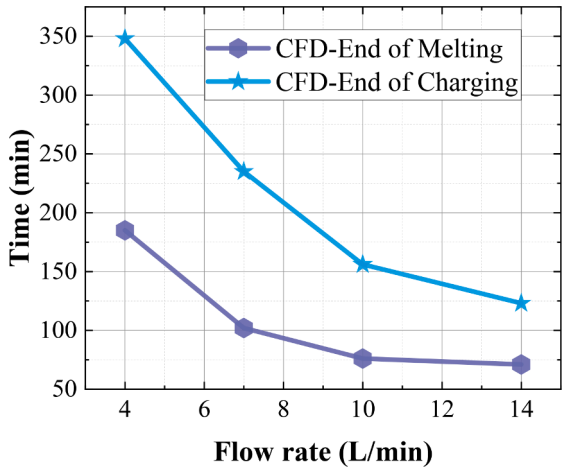

Fig. 16. The melting and charging time of calculated results.

was obviously limited by the tank size.

Table 2 listed all the thermal characteristics during charge under different flow rate conditions. The full charge time decreases with the increase of the flow rate. This means though the size of the tank limited the heating inside the tank, increasing the flow rate can still shorten the full charge time. When the tank was fully charged, it needs 21.4–22.0 kWh heat from heat source under different flow rate conditions. The needed energy was related to heating duration, heat loss and the temperature distribution inside the tank. When using the flow rate of 10 L/min, the tank only needs 21.4 kWh energy to be fully charged.

In the charging process, increasing the flow rate is an efficient method to increase the thermal performance of the tank. But increasing the flow rate means additional energy cost for pumping. The gain of increasing flow rate decreases as the flow rate increases.

4.4.2.2. Discharge of the sensible heat. Fig. 18 shows the power and *HXCR* of the tank during discharge of the sensible heat. As the discharge goes on, under all flow rate conditions, both power and *HXCR* decreased. The influence of flow rate on discharging process is obvious. Both power and *HXCR* increased with the increase of flow rate.

Table 3 listed the value of the thermal characteristics during discharge of sensible heat process under different flow rate conditions. With the flow rate increased from 4 L/min to 14 L/min, the energy weighted discharge power increased from 14.3 kW to 41.6 kW (191%), the energy weighted *HXCR* increased from 657 W/K to 807 W/K (23%). The average temperature of the produced hot water decreased from 77.5 °C to 68.2 °C. Increasing the flow rate can shorten the hot water producing time efficiency from 61 min to 21 min. The maximum hot water (294 L) was produced by the heat storage for 14 L/min.

4.4.2.3. Discharge of the latent heat. Fig. 19 shows the power and *HXCR* of the tank during the discharge of the latent heat process. After triggering the solidification of the supercooled PCM, the process of discharging latent heat is similar to the process of discharging sensible heat. Power and *HXCR* decreased with the development of discharging. When increasing the flow rate, the discharge power and *HXCR* increased.

Table 4 listed the value of the thermal characteristics during discharge of the latent heat process under different flow rate conditions. With the increase of flow rate, the energy weighted power and energy weighted *HXCR* increased from 5.3 kW to 12.3 kW and 493 W/K to 612 W/K. The average temperature and time of produced hot water decreased from 50.0 °C to 45.2 °C and 76 min to 13 min respectively. One interesting point is, the maximum volume of produced hot water (334 L) occurred for 10 L/min.

It can be concluded that the inlet flow rate has obvious influences on the thermal characteristics of the heat storage in both the charging and discharging process. The influence may be limited by the size of the tank. If the size limitation is ignored, increasing the flow rate is an efficient way to enhance the heat transfer inside the tank.

Conclusion

A flexible thermal energy storage was investigated by experiments and CFD simulations. 137.8 kg PCM and 75 L water were filled in the heat storage. The flexible heat storage combined short-term and long-term heat storage functions. Under the experimental conditions, after fully charged, the heat storage can release heat in two steps: In the first

Table 2
Thermal characteristics of the tank during charging.

Flow rate	P^1	$HXCR^2$	Full Charge	
			Time[3]	Needed Energy
L/min	kW	W/K	min	kWh
4	6.1	170	276	22.0
7	11.4	390	152	21.6
10	16.4	520	108	21.4
14	18.1	466	92	21.6

[1] Energy weighted power.
[2] Energy weighted *HXCR*.
[3] The time for heating all PCM to be higher than 87 °C.

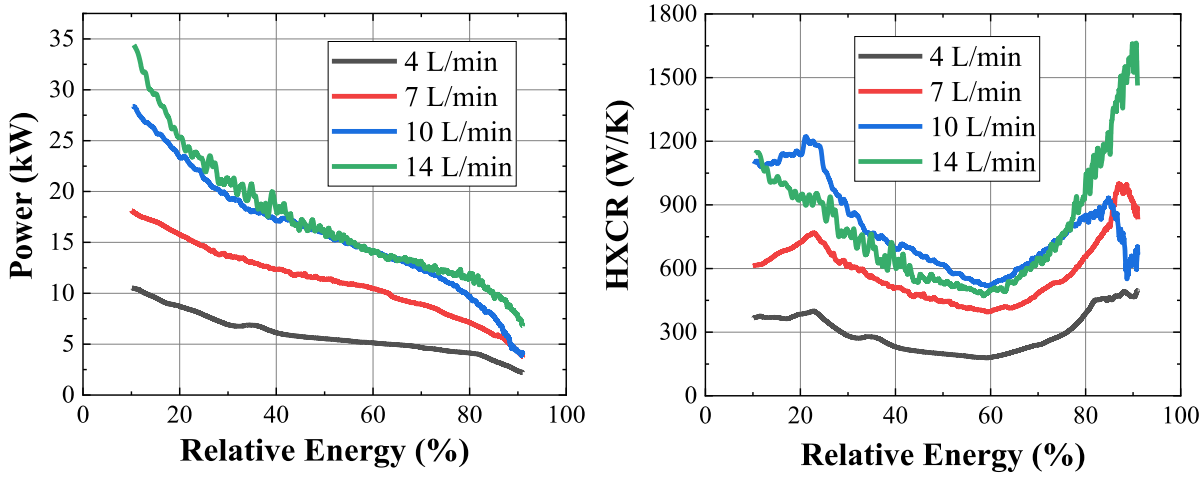

Fig. 17. Power and *HXCR* in the charging process.

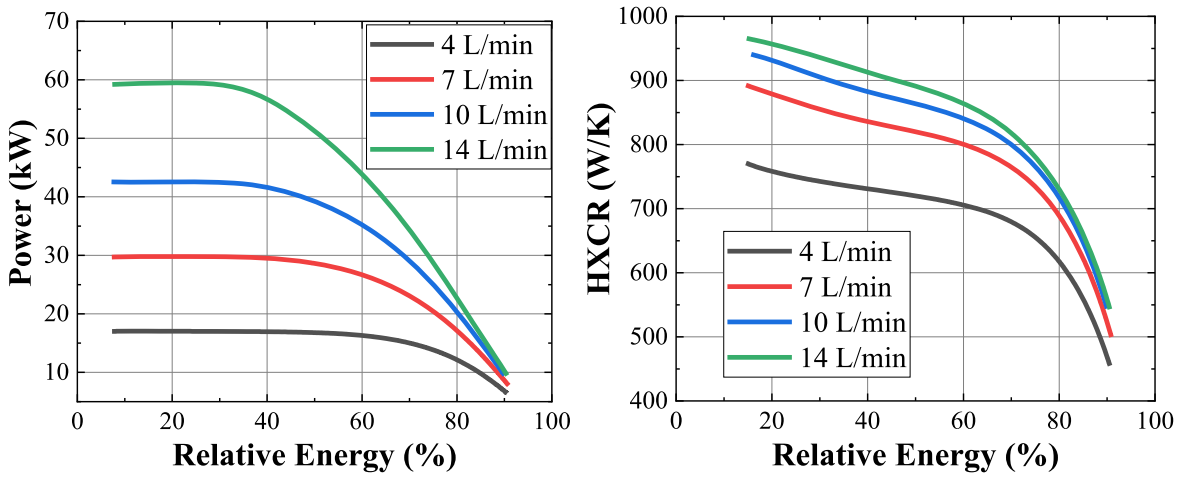

Fig. 18. Power and *HXCR* in discharging of sensible heat process.

Table 3
Thermal characteristics of the tank during discharging of sensible heat process.

Flow rate	P^1	$HXCR^2$	Produced Hot water		
			Volume	Average T	Time
L/min	kW	W/K	L	°C	min
4	14.3	657	244	77.5	61
7	23.6	750	252	74.4	36
10	31.9	786	260	72.0	26
14	41.6	807	294	68.2	21

[1] Energy weighted power.
[2] Energy weighted *HXCR*.

step, 13.7 kWh sensible heat was released as short-term heat storage; in the second step, 7.8 kWh latent heat can be released on demand as long-term heat storage.

The developed CFD model can accurately simulate the melting process, supercooling process and solidification process of the heat storage. The maximum difference between the calculated and the measured power transfers to and from the heat storage was less than 3%.

The flow characteristics of water and liquid PCM were revealed by the CFD calculations. The flow pattern in the tank during the discharging processes was unchanged, no matter if the sensible heat or the latent heat is released. The thermal stratification inside the water was obvious, the water can be effectively heated by PCM tubes. In the discharging of the sensible heat process, the heat storage can produce 294 L hot water (68.2 °C average temperature). In discharging of the latent heat process, the produced water was 334 L (46.7 °C average temperature).

In the charging process, the fluid short circuit existed inside the water region. Part of the incoming hot water flows out of the tank without sufficient release of heat. There was no obvious thermocline inside the tank during charging. Some tubes were heated directly by hot water, other tubes were heated by the reverse flow. For 10 L/min flow rate, 16 tubes in the heat storage were directly heated. The non-uniform heating phenomenon should be further investigated in future investigations. Potential remedy could be regulation of the incoming flow by adding baffles or a flow equalizing plate.

The flow rate obviously influenced the thermal characteristics of the heat storage. During charge, when the flow rate increased from 4 L/min

Table 4
Thermal characteristics of the tank during discharging of latent heat process.

Flow rate	P^1	$HXCR^2$	Produced Hot water		
			Volume	Average T	Time
L/min	kW	W/K	L	°C	min
4	5.3	493	306	50.0	76
7	8.1	553	324	48.2	46
10	10.3	586	334	46.7	33
14	12.3	612	329	45.2	13

[1] Energy weighted power.
[2] Energy weighted *HXCR*.

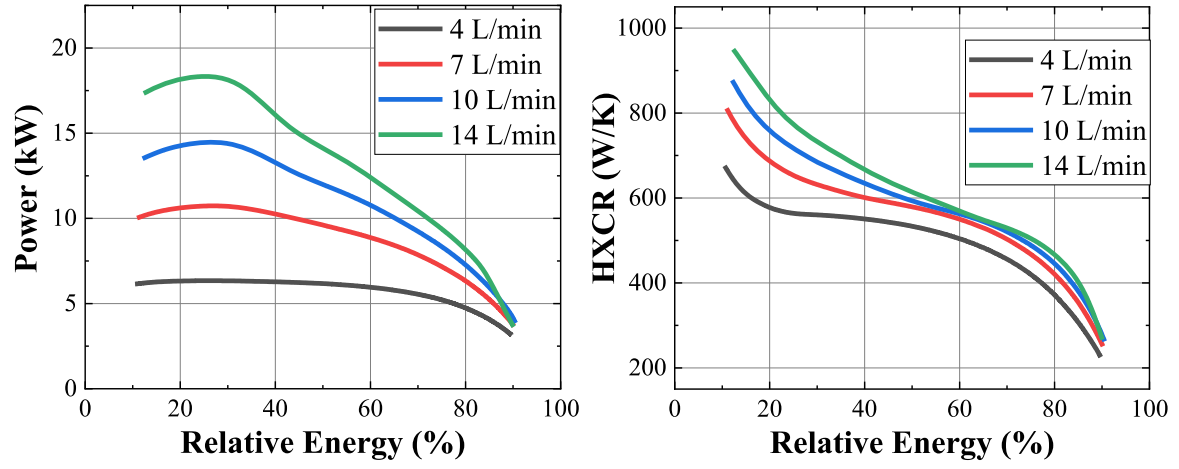

Fig. 19. The power and *HXCR* during discharging of latent heat process.

to 14 L/min, the charging process can be effectively shortened by 67% (from 276 min to 92 min), and the temperature distribution of water becomes more uniform. During discharging, increasing the flow rate can also enhance the heat transfer inside the tank. For discharging of sensible heat, when the flow rate increased from 4 L/min to 14 L/min, the discharging time decreased from 61 min to 21 min. Similarly, for discharging of latent heat, it decreased from 76 min to 13 min.

Power and *HXCR* was influenced by the flow rate obviously. Generally, the power and *HXCR* of the heat storage increased with the increase of flow rate when ignoring the limitation of the tank size. In charge process, the maximum charging power and *HXCR* were 18.1 kW and 520 W/K respectively. In discharge of the sensible heat process, the maximum discharging power and *HXCR* was 41-.6 kW and 807 W/K. In discharge of latent heat process, they were 12.3 kW and 612 W/K respectively.

CRediT authorship contribution statement

Gang Wang: Formal analysis, Methodology, Validation, Visualization, Writing – original draft. **Chao Xu:** Writing – review & editing. **Gerald Englmair:** Writing – review & editing. **Weiqiang Kong:** Writing – review & editing. **Jianhua Fan:** Funding acquisition, Project administration, Resources, Supervision, Writing – review & editing. **Simon Furbo:** Writing – review & editing. **Gaosheng Wei:** Writing – review & editing.

Declaration of Competing Interest

The authors declare that they have no known competing financial interests or personal relationships that could have appeared to influence the work reported in this paper.

Acknowledgments

The research was financed by the Danish Energy Agency EUDP project on participation of the IEA Task 58 'Material and Component Development for Thermal Energy Storage'. The research was partly funded by H.M. Heizkörper GmbH Heating Technology & Co. KG who developed the heat storage unit prototypes, partly supported by the National Natural Science Foundation of China (No. 51821004) as well as the Fundamental Research Funds for the Central Universities (No. 2019QN036).

References

[1] D. Icaza, D. Borge-diez, S. Pulla, Proposal of 100% renewable energy production for the City of Cuenca- Ecuador by 2050, Renew. Energy 170 (2021) 1324–1341, https://doi.org/10.1016/j.renene.2021.02.067.

[2] T. Xiong, L. Zheng, K.W. Shah, Nano-enhanced phase change materials (NePCMs): a review of numerical simulations, Appl. Therm. Eng. 178 (2020), 115492, https://doi.org/10.1016/j.applthermaleng.2020.115492.

[3] R. Heffron, S. Halbrügge, M.F. Körner, N.A. Obeng-Darko, T. Sumarno, J. Wagner, M. Weibelzahl, Justice in solar energy development, Sol. Energy 218 (2021) 68–75, https://doi.org/10.1016/j.solener.2021.01.072.

[4] Y. Heng, C. Lu, L. Yu, Z. Gao, The heterogeneous preferences for solar energy policies among US households, Energy Policy 137 (2020), 111187, https://doi.org/10.1016/j.enpol.2019.111187.

[5] Q. Li, C. Li, Z. Du, F. Jiang, Y. Ding, A review of performance investigation and enhancement of shell and tube thermal energy storage device containing molten salt based phase change materials for medium and high temperature applications, Appl. Energy (2019), https://doi.org/10.1016/j.apenergy.2019.113806.

[6] M. Caliano, N. Bianco, G. Graditi, L. Mongibello, Analysis of a phase change material-based unit and of an aluminum foam/phase change material composite-based unit for cold thermal energy storage by numerical simulation, Appl. Energy 256 (2019), 113921, https://doi.org/10.1016/j.apenergy.2019.113921.

[7] Z. Yu, D. Gibbs, Encircling cities from rural areas ? Barriers to the di ff usion of solar water heaters in China' s urban market, Energy Policy 115 (2018) 366–373, https://doi.org/10.1016/j.enpol.2018.01.041.

[8] S. Shaikh, K. Lafdi, C/C composite, carbon nanotube and paraffin wax hybrid systems for the thermal control of pulsed power in electronics, Carbon N. Y. 48 (2010) 813–824, https://doi.org/10.1016/j.carbon.2009.10.034.

[9] Z. Liu, S. Zhang, D. Hu, Y. Zhang, H. Lv, C. Liu, Y. Chen, J. Sun, Paraffin/red mud phase change energy storage composite incorporated gypsum-based and cement-based materials: microstructures, thermal and mechanical properties, J. Hazard. Mater. 364 (2019) 608–620, https://doi.org/10.1016/j.jhazmat.2018.10.061.

[10] C. Zauner, F. Hengstberger, M. Etzel, D. Lager, R. Hofmann, H. Walter, Experimental characterization and simulation of a fin-tube latent heat storage using high density polyethylene as PCM, Appl. Energy 179 (2016) 237–246, https://doi.org/10.1016/j.apenergy.2016.06.138.

[11] P. Kumar, S. Rathore, S.K. Shukla, Energy & Buildings Enhanced thermophysical properties of organic PCM through shape stabilization for thermal energy storage in buildings : a state of the art review, Energy Build. 236 (2021), 110799, https://doi.org/10.1016/j.enbuild.2021.110799.

[12] K. Du, J. Calautit, P. Eames, Y. Wu, A state-of-the-art review of the application of phase change materials (PCM) in mobilized-thermal energy storage (M-TES) for recovering low-temperature industrial waste heat (IWH) for distributed heat supply, Renew. Energy 168 (2021) 1040–1057, https://doi.org/10.1016/j.renene.2020.12.057.

[13] Y. Wang, K. Yu, H. Peng, X. Ling, Preparation and thermal properties of sodium acetate trihydrate as a novel phase change material for energy storage, Energy 167 (2019) 269–274, https://doi.org/10.1016/j.energy.2018.10.164.

[14] S.M. Shalaby, A.E. Kabeel, B.M. Moharram, A.H. Flea, Experimental study of the solar water heater integrated with shell and fi nned tube latent heat storage system, 31 (2020). 10.1016/j.est.2020.101628.

[15] B. Lamrani, Thermal performance of a coupled solar parabolic trough collector latent heat storage unit for solar water heating in large buildings d e, 162 (2020). 10.1016/j.renene.2020.08.038.

[16] Y. Qin, Z. Wang, H. Zhang, B. Dou, G. Zhang, W. Wu, C. Wu, The effect of phase change material balls on the thermal characteristics in hot water tanks: CFD research, Appl. Therm. Eng. (2020) 178, https://doi.org/10.1016/j.applthermaleng.2020.115557.

[17] Y. Bai, Z. Wang, J. Fan, M. Yang, Numerical and experimental study of an underground water pit for seasonal heat storage, Renew. Energy 150 (2020) 487–508, https://doi.org/10.1016/j.renene.2019.12.080.

[18] J. Xu, R.Z. Wang, Y. Li, A review of available technologies for seasonal thermal energy storage, Sol. Energy 103 (2014) 610–638, https://doi.org/10.1016/j.solener.2013.06.006.

[19] Z. Tian, S. Zhang, J. Deng, J. Fan, J. Huang, W. Kong, B. Perers, S. Furbo, Large-scale solar district heating plants in Danish smart thermal grid: developments and recent trends, Energy Convers. Manag. 189 (2019) 67–80, https://doi.org/10.1016/j.enconman.2019.03.071.

[20] K. Narula, F. De Oliveira, W. Villasmil, M.K. Patel, Simulation method for assessing hourly energy fl ows in district heating system with seasonal thermal energy storage, Renew. Energy 151 (2020) 1250–1268, https://doi.org/10.1016/j.renene.2019.11.121.

[21] A. Dahash, F. Ochs, A. Tosatto, W. Streicher, Toward efficient numerical modeling and analysis of large-scale thermal energy storage for renewable district heating, Appl. Energy 279 (2020), 115840, https://doi.org/10.1016/j.apenergy.2020.115840.

[22] H. Gadd, S. Werner, Thermal Energy Storage Systems for District Heating and Cooling, 21, LTD, 2021, https://doi.org/10.1016/B978-0-12-819885-8.00021-8.

[23] G. Zhou, M. Zhu, Y. Xiang, Effect of percussion vibration on solidification of supercooled salt hydrate PCM in thermal storage unit, Renew. Energy 126 (2018) 537–544, https://doi.org/10.1016/j.renene.2018.03.077.

[24] G. Zhou, Y. Xiang, Experimental investigations on stable supercooling performance of sodium acetate trihydrate PCM for thermal storage, Sol. Energy 155 (2017) 1261–1272, https://doi.org/10.1016/j.solener.2017.07.073.

[25] W. Kong, M. Dannemand, J.B. Johansen, J. Fan, J. Dragsted, G. Englmair, S. Furbo, Experimental investigations on heat content of supercooled sodium acetate trihydrate by a simple heat loss method, Sol. Energy 139 (2016) 249–257, https://doi.org/10.1016/j.solener.2016.09.045.

[26] G. Wang, M. Dannemand, C. Xu, G. Englmair, S. Furbo, J. Fan, Thermal characteristics of a long-term heat storage unit with sodium acetate trihydrate, Appl. Therm. Eng. 187 (2021), 116563, https://doi.org/10.1016/j.applthermaleng.2021.116563.

[27] M. Dannemand, J.B. Johansen, W. Kong, S. Furbo, Experimental investigations on cylindrical latent heat storage units with sodium acetate trihydrate composites utilizing supercooling, Appl. Energy 177 (2016) 591–601, https://doi.org/10.1016/j.apenergy.2016.05.144.

[28] G. Englmair, C. Moser, S. Furbo, M. Dannemand, J. Fan, Design and functionality of a segmented heat-storage prototype utilizing stable supercooling of sodium acetate trihydrate in a solar heating system, Appl. Energy 221 (2018) 522–534, https://doi.org/10.1016/j.apenergy.2018.03.124.

[29] M. Dannemand, J.M. Schultz, J.B. Johansen, S. Furbo, Long term thermal energy storage with stable supercooled sodium acetate trihydrate, Appl. Therm. Eng. 91 (2015) 671–678, https://doi.org/10.1016/j.applthermaleng.2015.08.055.

[30] G. Englmair, C. Moser, H. Schranzhofer, J. Fan, S. Furbo, A solar combi-system utilizing stable supercooling of sodium acetate trihydrate for heat storage: numerical performance investigation, Appl. Energy 242 (2019) 1108–1120, https://doi.org/10.1016/j.apenergy.2019.03.125.

[31] F. Mohammadnejad, S. Hossainpour, A CFD modeling and investigation of a packed bed of high temperature phase change materials (PCMs) with different layer configurations, J. Energy Storage 28 (2020), 101209, https://doi.org/10.1016/j.est.2020.101209.

[32] T. Bouhal, S. ed-Dîn Fertahi, T. Kousksou, A. Jamil, CFD thermal energy storage enhancement of PCM filling a cylindrical cavity equipped with submerged heating

sources, J. Energy Storage 18 (2018) 360–370, https://doi.org/10.1016/j.est.2018.05.015.

[33] V.R. Pawar, S. Sobhansarbandi, CFD modeling of a thermal energy storage based heat pipe evacuated tube solar collector, J. Energy Storage 30 (2020), 101528, https://doi.org/10.1016/j.est.2020.101528.

[34] M. Dannemand, J. Fan, S. Furbo, J. Reddi, Validation of a CFD model simulating charge and discharge of a small heat storage test module based on a sodium acetate water mixture, Energy Procedia 57 (2014) 2451–2460, https://doi.org/10.1016/j.egypro.2014.10.254.

[35] Simon Furbo, Varmelagring Til Solvarmeanlæg Link back to DTU Orbit, Tech. Univ. Denmark. Thermal, 1984.

[36] Ansys.Inc, Ansys engineering simulation softwares, 2021 (n.d.). https://www.ansys.com/en-gb.

[37] T. Bouhal, Z. Meghari, S. ed D. Fertahi, T. El Rhafiki, T. Kousksou, A. Jamil, E. Ben Ghoulam, Parametric CFD analysis and impact of PCM intrinsic parameters on melting process inside enclosure integrating fins: solar building applications, J. Build. Eng. 20 (2018) 634–646, https://doi.org/10.1016/j.jobe.2018.09.016.

[38] W. Youssef, Y.T. Ge, S.A. Tassou, CFD modelling development and experimental validation of a phase change material (PCM) heat exchanger with spiral-wired tubes, Energy Convers. Manag. 157 (2018) 498–510, https://doi.org/10.1016/j.enconman.2017.12.036.